

Ambipolar field-effect transistor on as-grown single-wall carbon nanotubes

Bakir Babić, Mahdi Iqbal and Christian Schönenberger¹

Institut für Physik, Universität Basel, Klingelbergstraße 82, CH-4056 Basel, Switzerland

E-mail: Christian.Schönenberger@unibas.ch

Received 28 August 2002, in final form 23 December 2002

Published 28 January 2003

Online at stacks.iop.org/Nano/14/327

Abstract

We use a simultaneous flow of ethylene and hydrogen gases to grow single-wall carbon nanotubes by chemical vapour deposition. Strong coupling to the gate is inferred from transport measurements for both metallic and semiconducting tubes. At low temperatures, our samples act as single-electron transistors where the transport mechanism is mainly governed by Coulomb blockade. The measurements reveal very rich quantized energy level spectra spanning from the valence to the conduction band. The Coulomb diamonds have similar addition energies on both sides of the semiconducting gap. Signatures of the subband population have been observed at intermediate temperature.

1. Introduction

Single-wall carbon nanotubes (SWNTs) are chemically derived self-assembled solid molecules with fascinating electronic properties [1]. Their rich variety of band structure (metallic, semiconductor) might revolutionize nanoelectronics. Recently, not only has an extensive spectrum of quantum phenomena been demonstrated with SWNTs [2–5], but they have also been used as functional electronic devices in the form of field effect transistors (FETs) [6, 7]. The as-grown SWNT FETs were found to be unipolar p-type, i.e. no electrical current flows even at large positive gate voltages. The p-type nature of nanotubes (NTs) has been attributed to charge transfer caused by either oxidizing molecules adsorbed to the NTs [8], or the difference in workfunctions between NTs and metallic contacts [6]. The unipolarity, on the other hand, has been attributed to the presence of Schottky barriers at the metal–nanotube contacts [9]. Though as-grown SWNTs are p-type, n-type unipolar conductance has been demonstrated by either chemical doping [10] or an annealing treatment in an inert environment [11]. It remains, however, challenging to realize *as-grown* ambipolar SWNT FETs with conventional back-gates. Ambipolar SWNT FETs have been demonstrated on large-diameter SWNTs (3–5 nm) [12], and recently also on small-diameter SWNTs (1–2 nm) by using strong-coupling gates [13]. Here we report on electric transport measurements of as-grown SWNTs which display ambipolar FET action.

¹ Author to whom any correspondence should be addressed.

2. Experiment

SWNTs are synthesized by chemical vapour deposition (CVD) following the method of Hafner *et al* [14]. In all our studies we used SWNTs having diameters of 2 nm or less, as inferred from atomic force microscopy (AFM) height measurements. Our devices are prepared on highly doped ($<0.02 \Omega \text{ cm}$) and thermally oxidized (400 nm) Si wafers. The substrate is used as the back-gate in electrical measurements of the final devices which are obtained as follows: the substrate is covered with a layer of polymethylmethacrylate (PMMA) in which windows ($5 \times 10 \mu\text{m}^2$) are patterned by electron beam lithography. Then, a catalyst suspension consisting of 1 mg iron nitrate seeds ($\text{Fe}(\text{NO}_3)_3$) dissolved in 10 ml of isopropanol is poured into the predefined trenches. The PMMA is then removed in acetone, leaving isolated catalyst islands on the surface. The CVD growth is performed in a quartz-tube furnace at 800 °C and atmospheric pressure using a gas mixture of ethylene, hydrogen and argon with respective flow rates of 2, 400 and 600 $\text{cm}^3 \text{min}^{-1}$. During heating and cooling of the furnace, the quartz tube is continually flashed with argon to avoid contamination of the tubes. The as-grown SWNTs are then contacted in a conventional lift-off process with two metal electrodes per SWNT, spaced 1 μm apart. As electrode material a bilayer of Ti (2 nm) and Au (60 nm) is used, leading to contact resistances of $\approx 40 \text{ k}\Omega$ at room temperature. Figure 1(a) illustrates schematically a SWNT device. An AFM picture is displayed in figure 1(b). The

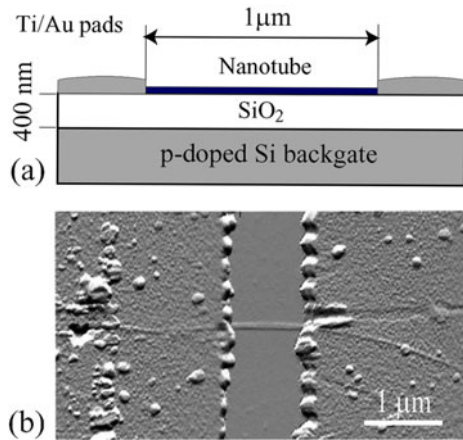


Figure 1. (a) Scheme of an SWNT device contacted by two Ti/Au electrodes. The Si substrate is used as the back-gate. (b) AFM image of an SWNT bridging between the two electrodes.

diameter of the nanotubes is determined from the measured height using AFM in tapping mode.

3. Results and discussion

Once the samples are made, semiconducting and metallic tubes are distinguished by the dependence of their electrical conductance G on the gate voltage V_g , measured in a wide temperature range of 0.3–300 K. Figure 2 shows a measurement of the linear conductance $G(V_g)$ for a semiconducting SWNT at moderate temperatures of $T = 40$ and 60 K, respectively. Starting from $V_g = -10$ V G decreases with increasing V_g , indicating p-type behaviour, while above $V_g \approx 4$ V G increases, indicating n-type behaviour. In between these two regions the conductance is low, which suggests carrier depletion. This low conductance region therefore corresponds to the gap [12, 15]. The charge-neutrality point for this sample lies at $V_g = 2.5$ V. It varies in general between $V_g = -2.5$ and 2.5 eV. Our finding demonstrates that as-grown SWNTs can be ambipolar transistors.

$G(V_g)$ is slightly lower at 40 than at 60 K. If the temperature is lowered further, the linear-response conductance is suppressed further to eventually become very small. This is caused by Coulomb interaction, which first results in a power-law suppression of G with T [4, 16] and at low temperatures in the emergence of Coulomb blockade (CB). The latter is observed and will be discussed afterwards.

The two-terminal resistance R of a carbon-nanotube device has two parts: the resistance arising from the contacts and a finite mobility (resistivity) of the NT. The relative magnitude is currently discussed. One prominent school of scientists assigns the major part of R to Schottky barriers at the contacts impeding transport and provides some evidence in favour of it [7, 17, 18]. However, the discussed devices have resistances in the range of 1–100 M Ω , i.e. are rather high ohmic. The device which we show in figure 2 has a lower resistance, of order 0.1 M Ω . Assuming that the conductance of this devices is limited by scattering within the NT, the mobility μ can be estimated taking a linear approximation of $G(V_g)$ (dashed curves in figure 2). This yields a relatively high average carrier mobility of $\mu \approx 800$ cm² V⁻¹ s⁻¹. The mobility can be related to the 1D diffusion coefficient

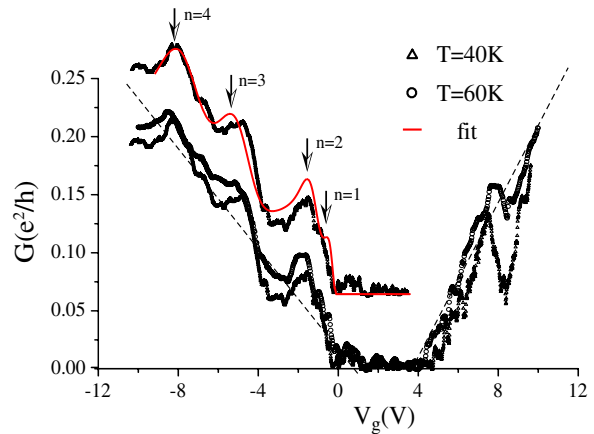


Figure 2. Two-terminal (linear) conductance G as a function of gate voltage V_g for a semiconducting SWNT at moderate temperatures of $T = 40$ and 60 K, respectively. The peaks in G are attributed to VHS in the one-dimensional DOS. A respective fit to the $T = 40$ K data is shown as a solid curve (shifted vertically for clarity).

(This figure is in colour only in the electronic version)

$D = v_F l$ via $D = \mu E_F / e$, where E_F is the Fermi energy, $v_F \approx 10^6$ m s⁻¹ the Fermi velocity and l the scattering mean free path. Taking the approximation $E_F \approx 0.5$ eV yields $D \approx 0.4$ m² s⁻¹ and $l \approx 40$ nm. Note that this estimate results in lower bounds for μ , D and l , because of (the unknown) contribution to the total resistance from the contacts.

$G(V_g)$ is not strictly linear, but shows several pronounced humps, suggestive of van Hove singularities (VHSs) in the density of states (DOS) of the one-dimensional (1D) bandstructure of NTs. The conductance G is proportional to the 1D DOS N_{1D} , both in the case of tunnelling and low-ohmic contacts, provided the band structure moves rigidly with the gate voltage (no Fermi-level pinning). The proportionality coefficient is then determined by the tunnelling coupling parameter or the diffusion coefficient, respectively. To test this scenario, we have modelled $G(V_g)$ by $G(V_g) \propto N_{1D}(E(V_g))$ and display a fit to the curve at $T = 40$ K on the p-side in figure 2 (shifted vertically for clarity). There are three fitting parameters: the energy broadening δ , the gate capacitance C_g and the prefactor between N_{1D} and G . δ is determined to be 0.13 eV. This is reasonable if we compare with the inverse scattering time, given by $v_F h / l \approx 0.1$ eV. C_g determines the horizontal scale of the plot and the prefactor the diffusion coefficient (or the tunnelling coupling, if tunnelling contacts are assumed to dominate the resistance). We will discuss these scaling parameters (in particular the gate coupling) later, after having introduced the low-temperature measurements.

In fitting the measurement we have used a regular sequence of 1D subbands with threshold energies of $E/E_0 = 1, 2, 4, 5$. The respective van Hove peaks are marked by arrows in figure 2. Note that the first VHS is hardly visible and that the peak spacing on the gate-voltage axis is modified. The latter apparent change is caused by the non-linear E_F versus V_g dependence. We have obtained this dependence assuming that a gate-voltage change leads to charging of the gate capacitance C_g connected in series with the electrochemical capacitance of the NT [19]. The latter is given by the DOS. To first order (averaging over VHS) we obtain $E_F \propto \sqrt{V_g}$.

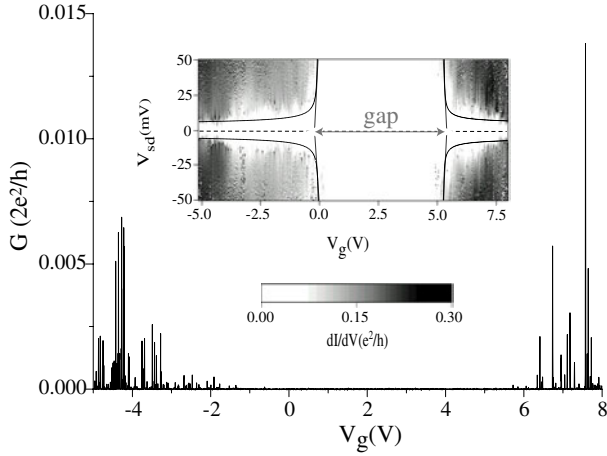


Figure 3. Linear conductance G as a function of gate voltage V_g (main plot) and greyscale representation of the differential conductance dI/dV as a function of V_g and applied source–drain voltage V_{sd} (inset) at 2 K for an SWNT device. White regions correspond to zero and dark regions to high conductances (maximum $0.3 e^2/h$). The semiconducting gap is clearly visible as a large non-conducting region in the inset. Coulomb oscillations peaks are observed on the p (left) and n (right) sides of the semiconducting gap.

We now turn to low-temperature measurements $T \leq 4$ K. Figure 3 shows $G(V_g)$ and a greyscale representation (inset) of the differential conductance dI/dV as a function of V_g and applied transport voltage V_{sd} of an SWNT device at $T = 2$ K. The large white zone in the middle of the greyscale plot corresponds to a non-conducting region related to the semiconducting gap. The thick lines drawn at the edges are guides to the eye. Their vertical extensions intersect around $V_{sd} \cong 0.6$ eV, which is a direct estimate of the gap energy. On both sides of the gap Coulomb blockade diamonds (CBDs) of varying size are observed (we refer to the term ‘diamond’, although the blockade region is not composed of a series of neat diamonds). Though the addition energy E_{add} (sum of single-electron charging energy and level spacing) is seen to fluctuate in between 2.5 mV and $\lesssim 20$ meV, there is a general trend, indicated by the thin curved lines. Close to the gap, E_{add} is large and decays to a smaller value for lower (higher) V_g on the p (n) side. This is not expected for an ideal (*defect-free*) semiconducting NT for the following reason: at the onset of the conduction or valence band, the 1D DOS is expected to be large (VHS), since the band dispersion is parabolic to first approximation. If the NT can be considered as a single quantum dot extending from one contact to the other, the 0D level spacing δE should be very small, i.e. $\delta E = 0$ to first approximation. Provided the added charge can spread homogeneously along the whole tube, a constant charging energy U_c is expected. Hence, we would expect a constant addition energy in the case of an ideal defect-free tube, right at the edge of the gap. The observed discrepancy can be resolved (to some degree) if disorder is taken into account. Disorder will distribute the states over some energy interval leading to the observed broadening of the VHS, see figure 2. Moreover, this results in a smooth onset of the DOS and consequently in a relatively large 0D level-spacing δE . Disorder also (partially) localizes the wavefunctions, leading to both increased δE and U_c .

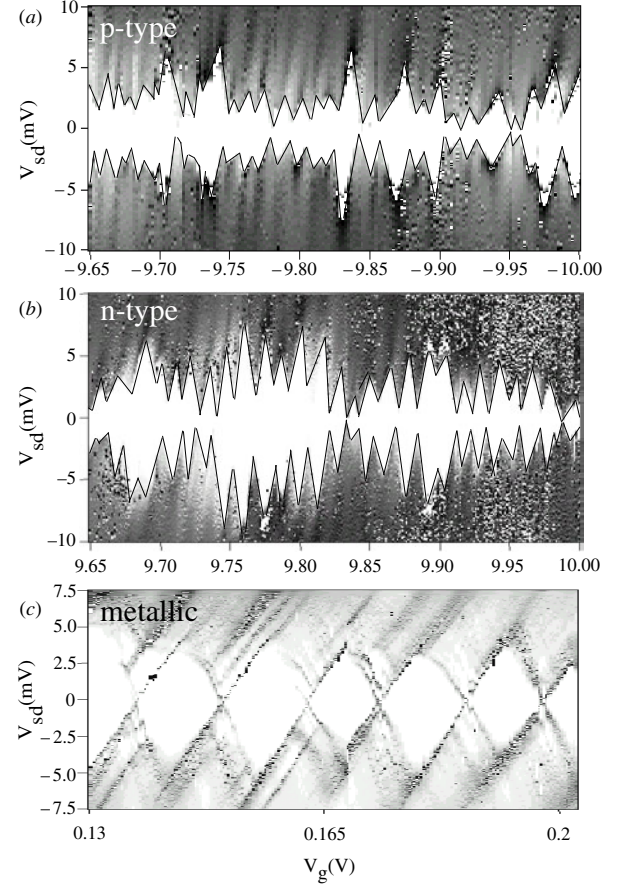


Figure 4. Differential conductance (dI/dV) plots as a function of V_g and V_{sd} . White corresponds to $dI/dV = 0$, and black to the maximum conductance of $0.3 e^2/h$. (a) and (b) have been measured on one semiconducting SWNT in the p region (a) and n region (b) at 2 K. As a reference a similar plot of another metallic SWNT measured at 0.3 K is shown in (c). While excited states can clearly be seen in (c), they appear to be absent in (a) and (b). Furthermore, while (c) displays a regular CB, it is irregular in (a) and (b). In all cases strong coupling to the gate is inferred.

Next, we focus on the region far away from the gap where ideally the 0D wavefunctions are extended, i.e. one quantum dot, and where the constant interaction model should yield a good approximation to single-electron charging effects. The charging energy is then given by the capacitances determined by the geometry of the device. Figure 4 presents three greyscale plots of the differential conductance dI/dV , 4(a) and (b) for one semiconducting NT and 4(c) for another metallic NT with identical contact spacing. The latter is shown as reference. Figures 4(a) and (b) correspond to conduction in the p and n region, respectively. Both have been measured around $|V_g| \approx 10$ V. If we compare with the metallic reference, the CB ‘diamonds’ are less regular in the semiconducting case, in particular most of the time they do not close. Importantly, however, they are similar in all respects on the n and p sides. The irregularity of the CB and the fact that the gap most often does not close implies that the NT does not act as a *single* quantum dot. The low maximum conductance of $\leq 0.025 e^2/h$ observed in the linear conductance in figure 3 supports this finding. Following the line pattern of conductance onset at finite V_{sd} , the addition energy E_{add} is given by the difference

between adjacent maxima and minima of V_{sd} . Hence, E_{add} varies in between ≈ 2 and 5 meV, as does the additional gap. This suggests that the NTs are split into two or at most three dots in series. The CB pattern on the n-side seems to show a beating pattern repeating after ≈ 6 –7 added charges. A strong beating pattern on the n-side has been observed before [15] and has been attributed to the formation of a small quantum dot in the vicinity of one of the contacts.

The analysis of Coulomb-blockade diamonds (CBD) permits us to extract the factor α [20] which measures the effectiveness of the coupling capacitance between the tube and the gate, i.e., $\alpha = C_g/C_\Sigma = U_c/\Delta V_g$. Here, C_g is the gate capacitance, C_Σ the total capacitance (gate plus contacts), $U_c = e^2/C_\Sigma$ the charging energy, and ΔV_g the single-electron period in gate voltage. We estimate the charging energy from the averaged value of the addition energy of a set of Coulomb diamonds. This results in $U_c \approx 2.5$ meV within a gate-voltage period of $\Delta V_g = 12$ mV, from which we deduce $\alpha \approx 0.2$. Note that this is a very high coupling efficiency for a nanotube whose gate electrode is as much as 400 nm away. Provided the constant-interaction model is valid in the semiconducting gap, we can predict the gap size, apparent in V_g . The gap in energy space is given by $E_{gap} = 4\hbar v_F/3d$, yielding 0.7 eV (the diameter d is taken to be $d = 1.2$ nm) [21]. Since the charging energy is negligibly small, $E_{add} = E_{gap}$. Multiplying with the ratio $\Delta V_g/U_c$ yields for the gap-size $\Delta V_{g-gap} = 3.4$ V, in reasonable agreement with the observed $\Delta V_{g-gap} \approx 4$ V in figure 2, or $\Delta V_{g-gap} \approx 5$ V in figure 3.

From α and U_c we obtain for the capacitances $C_g \approx 12.8$ aF and $C_\Sigma \approx 60$ aF. C_g is in reasonable agreement with the estimated geometrical capacitance $C_{geometry} = 2\pi L\epsilon_r\epsilon_0/\ln[2L/d]$ (L and d are the length and the diameter of the nanotube, respectively), yielding 29 aF. The factor of two difference most probably originates from the partial screening by the contacts.

The value of α found here is one of the largest values reported so far [11]. As a reference to our study on semiconducting SWNTs, we have investigated metallic tubes of similar length too. In contrast to semiconducting NTs regular CBDs are observed in metallic SWNTs (see figure 4(c)). At the edges of each diamond, parallel and sharp lines are visible reflecting excited states of the nanotube quantum dot. The charging energy and the single-electron level spacing are found to be 3 and 1 meV, respectively. The latter is in good agreement with the contact separation of $L \approx 1$ μm . This strongly suggests that metallic SWNTs behave like single quantum dots, unlike semiconducting SWNTs. In addition, the coupling to the gate $\alpha \sim 0.2$ –0.3 is equally large and corroborates the universal aspect of the high gate efficiency independent of the nature of the tubes.

Let us finally compare the horizontal axis (the gate voltage) of figure 4 ($T = 40, 60$ K) with figure 2 ($T = 2$ K). The low-temperature data allow us to count the added charge accurately. There are 30 electrons added in the gate-voltage interval shown in figures 4(a) and (b), leading to ≈ 100 electrons per 1 V. This capacitance value is obtained at a relatively high gate voltage of $|V_g| = 9.5$ –10 V. Referring to figure 2 and applying our assumption that the structure in G is due to the energy dependence of 1D subbands, we conclude that four subbands need to be occupied at this gate voltage.

The number of states per unit gate voltage at this Fermi-level (i.e. gate-voltage) position can be calculated and amounts to $\approx 5 \times 10^3 \text{ V}^{-1}$. Hence, we encounter a factor of 50 discrepancy! It may seem tempting to suggest another cause for the apparent oscillation of $G(V_g)$, namely CB oscillations. The period of CB oscillation of 3.5 V would correspond to a *very large* single-electron charging energy of $U_c \approx 0.4$ eV. If this were the case, G would be strongly suppressed even at $T = 60$ K, not to mention at 2 K. Note that the differential conductance is not suppressed if only a small source–drain voltage of a few millivolts is applied (see figure 3 (inset)), but is large, of order $0.3 e^2/h$. Therefore, CB can be disregarded as cause for the oscillation of $G(V_g)$ in figure 2. Since CB can be disregarded and because the 1D DOS in the fit of figure 2 reproduces the measurement very well, we think that the high-temperature data do reflect the 1D DOS. To get the number of states right, the resistance must be limited by a short section of the tube of length $1 \mu\text{m}/50 = 20$ nm, which in addition must be located close to or possibly even under the contacts in order to screen the Coulomb interaction. At lower temperature this short tube section is not visible in transport, because the resistance is then dominated by the CB of the whole NT. Apparent oscillations in $G(V_g)$ of SWNTs were assigned to the energy dependent 1D DOS by Liu *et al* [22]. However, no quantitative comparison with the expected DOS was performed.

4. Conclusions

In conclusion, we have shown that CVD-grown SWNTs, used as grown, can display high coupling strength to a back-gate. The strong coupling enables us to sweep the Fermi level continuously from p-to n-side, so that these FETs are ambipolar. At intermediate temperatures the overall two-terminal resistance R appears to be determined by a short tube segment close to the contacts, leading to the appearance of 1D DOS effects (VHS) in the linear conductance G versus gate voltage V_g . In contrast, at low temperature the average resistance R is higher and determined by the whole nanotube, notably by single-electron charging. The observed fluctuating addition energy points to disorder which (partially) splits the tube into one to three segments. As the maximum number of dots ≤ 3 at a contact separation of $L = 1$ μm , it appears that single quantum dots should be feasible at smaller contact separations ($L \lesssim 300$ nm). We emphasize that G can be swept from the p-to the n-side even at $T = 2$ K with no apparent barrier. As inferred from non-linear transport any barrier must be $\lesssim 2$ meV. Similarly low barriers were also observed in the work of Martel *et al* [17]. These authors argue that the barriers originate from the metal–nanotube contact and are Schottky barriers which are expected to be large, i.e. of order 0.3 eV. The observed conductance at low temperature can only be reconciled with large Schottky barriers if the barriers are so short that tunnelling through them is permitted. The band bending within a SWNT at the metallic contacts has been studied theoretically by Léonard and Tersoff [23]. It is concluded that the depletion region can be sufficiently short (< 5 Å) to permit sizable electron tunnelling, provided the doping fraction (or carrier density) of the NT is sufficiently large, i.e. $f \gtrsim 10^{-3}$. As an estimate, the carrier density at $V_g = 10$ V corresponds to a charge fraction of $f \approx 10^{-3}$,

which is in favour of short barriers. Similar doping densities were inferred from electrochemical gating experiments of MWNTs [19].

Acknowledgments

We acknowledge M R Buitelaar for fruitful discussions, T Nussbaumer for technical assistance and J Gobrecht for the Si substrates. This work is supported by COST (BBW), the NCCR on Nanoscience and the Swiss NFS.

References

- [1] See, e.g., Dresselhaus M S, Dresselhaus G and Eklund P C 1996 *Science of Fullerenes and Carbon Nanotubes* (New York: Academic)
- [2] Dekker C 1999 *Phys. Today* **52** 22
- [3] Kong J *et al* 2000 *Phys. Rev. Lett.* **87** 106801
- [4] Bockrath M, Cobden D H, Lu J, Rinzler A G, Smalley R E, Balents L and McEuen P L 1999 *Nature* **397** 598
- [5] Liang W, Bockrath M, Bozovic D, Hafner J H, Tinkham M and Park H 2001 *Nature* **411** 665
- [6] Tans S J, Verschueren A R M and Dekker C 1998 *Nature* **393** 49
- [7] Heinze S, Tersoff J, Martel R, Derycke V, Appenzeller J and Avouris Ph 2002 *Phys. Rev. Lett.* **89** 106801–1
- [8] Zhou C, Kong J, Yenilmez E and Dai H 2000 *Science* **290** 1552
- [9] Martel R, Schmidt T, Hertel T and Avouris P 1998 *Appl. Phys. Lett.* **73** 2447
- [10] Bockrath M, Hone J, Zettl A, McEuen P L, Rinzler A G and Smalley R E 2000 *Phys. Rev. B* **61** R10606
- [11] Radosavljević M, Feitag M, Thadani K V and Johnson A T 2002 *Nano Lett.* **2** 761
- [12] Javey A, Shim M and Dai H 2002 *Appl. Phys. Lett.* **80** 1064
- [13] Bachtold A, Hadley P, Nakanishi T and Dekker C 2001 *Science* **294** 1317
- [14] Hafner J H, Bronikowski M J, Azamian B R, Nikolaev P, Rinzler A G, Rinzler D T, Smith K A and Smalley R E 1998 *Chem. Phys. Lett.* **296** 195
- [15] Park J and McEuen P 2001 *Appl. Phys. Lett.* **79** 1363
- [16] Bachtold A, de Jonge M, Grove-Rasmussen K, McEuen P L, Buitelaar M R and Schönenberger C 2001 *Phys. Rev. Lett.* **87** 166801
- [17] Martel R, Derycke V, Lavoie C, Appenzeller R, Chan K K, Tersoff J and Avouris Ph 2001 *Phys. Rev. Lett.* **87** 256805
- [18] Freitag M, Radosavljević M, Zhou Y and Johnson A T 2001 *Appl. Phys. Lett.* **79** 3326
- Derycke V, Martel R, Appenzeller J and Avouris Ph 2002 *Appl. Phys. Lett.* **80** 2773
- Nakanishi T, Bachtold A and Dekker C 2002 *Phys. Rev. B* **66** 073307
- [19] Krüger M, Buitelaar M R, Nussbaumer T, Schönenberger C and Forró L 2001 *Appl. Phys. Lett.* **78** 1291
- [20] Beenakker C W J 1991 *Phys. Rev.* **44** 1646
- [21] Wildöer J W G, Venema L C, Rinzler A G, Smalley R E and Dekker C 1998 *Nature* **391** 59
- [22] Liu K, Burghard M, Roth S and Barnier P 1999 *Appl. Phys. Lett.* **75** 2494
- [23] Léonard F and Tersoff J 1999 *Phys. Rev. Lett.* **83** 5174
- Léonard F and Tersoff J 2000 *Phys. Rev. Lett.* **84** 4693